Journal of Sound and Vibration (2003) **259**(3), 701–710
doi:10.1006/jsvi.2002.5109, available online at http://www.idealibrary.com on IDEAL®

LETTERS TO THE EDITOR

ACTIVE CONTROL ON SOUND TRANSMISSION INTO AN ENCLOSURE THROUGH A FLEXIBLE BOUNDARY WITH EDGES ELASTICALLY RESTRAINED AGAINST TRANSLATION AND ROTATION

S. K. Lau and S. K. Tang

Department of Building Services Engineering, The Hong Kong Polytechnic University, Hung Hom, Hong Kong, China. E-mail: besltang@polyu.edu.hk

(*Received* 2 *January* 2002, *and in final form* 8 *April* 2002)

1. INTRODUCTION

Active control of sound transmission has been a subject of rigorous research in the past two decades. Typical examples include the works of Fuller and Jones [1], Qiu *et al.* [2], Pan *et al.* [3] and Pan and Hansen [4]. Also two control modes, namely the panel- and cavity-controlled modes, are found [3, 4]. The former refers to the case where the energy is transmitted from one dominating structural mode into several acoustic modes, while the latter concerns with the energy transfer from several structural modes into a single dominating acoustic mode. Kim [5] and Lau and Tang [6] analyzed this problem in a simplified form using the impedance-mobility approach.

In the present study, the influences of edge rotational and translational flexibilities on the active sound transmission control are discussed. The performance of active control using a pure vibration, a pure acoustic and combined secondary control sources under the potential energy control are studied. Full couplings between the boundary vibration and the enclosure acoustic modes are considered. For simplicity, a two-dimensional system is considered.

2. THE NUMERICAL MODEL

Computer simulation was performed to evaluate the effectiveness of the active sound transmission control in a two-dimensional rectangular enclosure as shown in Figure 1. The enclosure consists of three acoustically rigid walls and a flexible panel at $x_2 = 0$ whose edges are elastically restrained against rotation and translation. The dimensions of the enclosure, L_{x_1} (length) $\times$ L_{x_2} (width), were so chosen such that L_{x_1}: $L_{x_2} = 1$: e/π in order to reduce the number of degenerated acoustic modes. e denotes the exponential constant. According to Lau and Tang [6], the parameters, namely the strength of the structural–acoustic coupling, η_c, and the ratio between the first cut-off frequencies of the enclosure and the flexible panel, φ, can be defined as

$$\eta_c = \frac{\rho_a c^2 S_f}{\rho_s h V \omega_{ac} \omega_{sc}} \quad \text{and} \quad \varphi = \frac{\omega_{ac}}{\omega_{sc}}, \tag{1,2}$$

0022-460X/02/$35.00

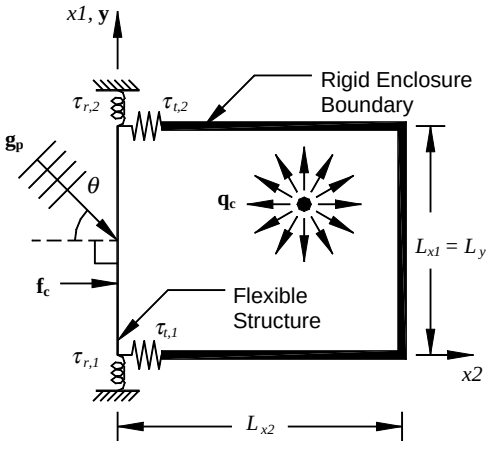

Figure 1. Schematic representation for sound transmission and the co-ordinate system adopted.

where ω_{ac} and ω_{sc} are the uncoupled first cut-off frequencies of the enclosure and simply supported flexible panel respectively. ρ_a and ρ_s are the densities of air and the flexible panel, respectively, c the speed of sound inside the enclosure and S_f the surface area of the flexible panel. V denotes the volume of the enclosure. The external modal force matrix, $\mathbf{g}_p$, on the flexible panel is induced by an external plane wave. It is estimated using the formula of Roussos [7]. Without loss of generality, the propagation direction of this wave is taken to be at $\theta = \pi/4$ in the present study. The force actuator and acoustic control source are located at $(0{\cdot}495L_{x_1}, 0)$ and (L_{x_1}, L_{x_2}), respectively, in order to avoid the nodal points on the panel and inside the enclosure throughout the frequency range considered in the present study. The optimal strengths of control sources under active control of sound transmission, the overall total acoustic potential energy and the sound pressure are determined using the normalized impedance-mobility approach [6] with acoustic and structural modal damping coefficients of 0.01.

The transverse vibration velocity, $\mathbf{u}_s$, at discrete points, $\mathbf{y}_i$, on an infinite long flexible panel, $\mathbf{u}_s = [u_s(\mathbf{y}_1, \hat{\omega})\, u_s(\mathbf{y}_2, \hat{\omega})\, u_s(\mathbf{y}_3, \hat{\omega}) \ldots]$, can be written as

$$\mathbf{u}_s = \mathbf{\Phi}^{\mathrm{H}}\mathbf{b}, \tag{3}$$

where $\mathbf{b}$ is the complex structural vibration velocity modal amplitude vector [6]. Each column of $\mathbf{\Phi}$ consists of M structural mode eigenfunctions, $\phi_m(\mathbf{y}_i)$, at a specified location, $\mathbf{y}_i$, on the flexible panel and

$$\phi_m(\mathbf{y}_i) = \alpha_{1,m}[\alpha_{2,m}\cosh(\lambda_m \mathbf{y}_i) + \alpha_{3,m}\sinh(\lambda_m \mathbf{y}_i) + \alpha_{4,m}\cos(\lambda_m \mathbf{y}_i) + \sin(\lambda_m \mathbf{y}_i)], \tag{4}$$

where $\alpha_{1,m}$, $\alpha_{2,m}$, $\alpha_{3,m}$, $\alpha_{4,m}$ and λ_m can be found with the system equation and the boundary conditions of edges elastically restrained against translation and rotation [8]:

$$D\frac{\partial^4 \phi_m(\mathbf{y})}{\partial \mathbf{y}^4} = j\rho_s h(\omega_{ac}\hat{\omega})^2 \phi_m(\mathbf{y}), \tag{5}$$

$$\frac{\partial \phi_m(0)}{\partial \mathbf{y}} = \tau_{r,1} D\frac{\partial^2 \phi_m(0)}{\partial \mathbf{y}^2}, \quad \phi_m(0) = -\tau_{t,1} D\frac{\partial^3 \phi_m(0)}{\partial \mathbf{y}^3}, \tag{6, 7}$$

and

$$\frac{\partial \phi_m(L_y)}{\partial \mathbf{y}} = -\tau_{r,2} D\frac{\partial^2 \phi_m(L_y)}{\partial \mathbf{y}^2}, \quad \phi_m(L_y) = \tau_{t,2} D\frac{\partial^3 \phi_m(L_y)}{\partial \mathbf{y}^3}, \tag{8, 9}$$

where D is the bending stiffness of the panel. $\tau_{r,i}$ and $\tau_{t,i}$ denote coefficients of the rotational and translational flexibility at each support respectively. The uncoupled normalized eigenfrequency of the flexible panel is given by

$$\hat{\omega}_m = \sqrt{\frac{D}{\rho_s h}} \frac{\lambda_m^2}{\omega_{sc}}, \tag{10}$$

Symmetric flexibility coefficients for both edges of the flexible panel are used in the present computation. Figure 2 shows the variation of the first three uncoupled normalized eigenfrequencies of the flexible panel at different edge flexibility coefficients for a 1 m long and 6 mm thick glass panel. $\hat{\omega}_{m=0} < 10^{-6}/\pi^2$ are neglected in the present calculation because there is no vibration at such small eigenfrequencies due to $\alpha_{2,m} \approx -\alpha_{4,m}$ and thus $\phi_m \approx 0$ as $\hat{\omega}_m \to 0$ (equations (4)–(9)). $\hat{\omega}_{m=1}$ reaches a plateau ($\hat{\omega}_{m=1} \approx 1$) for $\tau_t < 10^{-8}$ and decreases slightly for $\tau_t > 10^{-1}$. Also, it is nearly constant with $\tau_r < 10^{-6}$ and $\tau_r > 10$ for

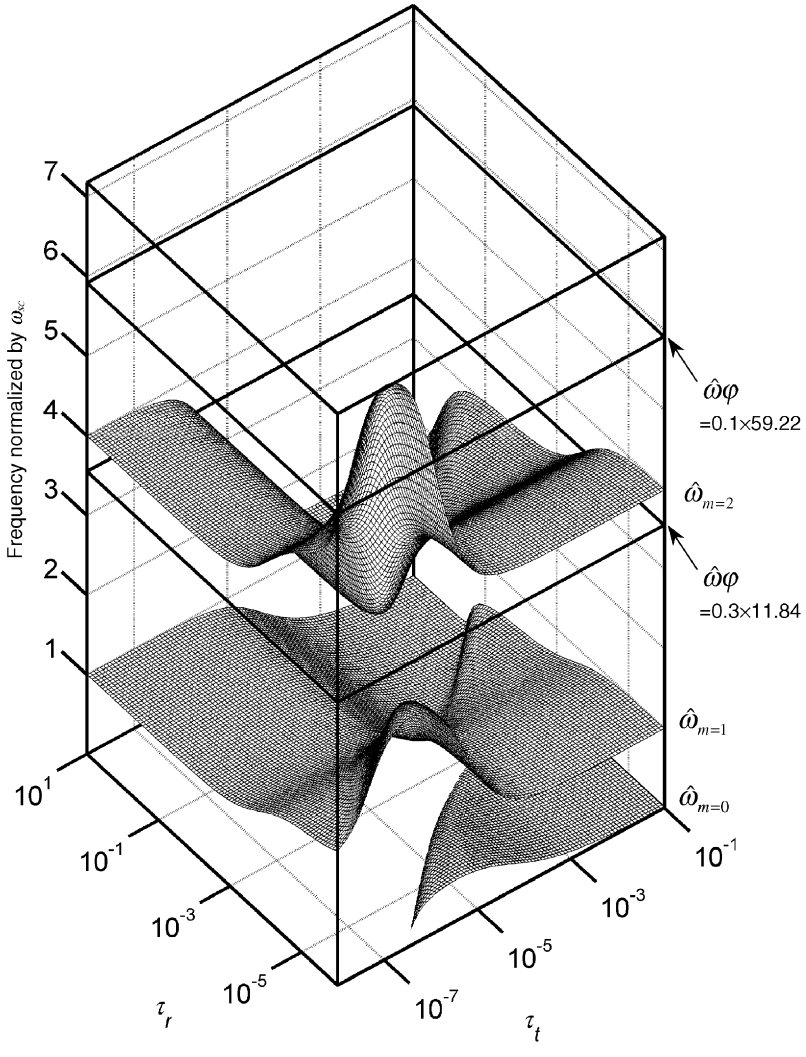

Figure 2. Variation of the first three eigenfrequencies of the flexible panel with τ_r and τ_t.

the range $10^{-8} < \tau_t < 10^{-1}$ except for small τ_r and τ_t. Similar profiles of $\hat{\omega}_m$ can be found for higher structural modes. Large variation of $\hat{\omega}_m$ can be found for the first few structural modes at different edge flexibility coefficients of the flexible panel, for instance, $\hat{\omega}_{m=2}$ as shown in Figure 2. However, the variation of $\hat{\omega}_m$ becomes smaller for higher structural modes with various flexibility coefficients (not shown here) because the structural mode shapes are less dependent on the boundary conditions of the flexible panel in these cases. In the present study, $10^{-6} < \tau_r < 10$ and $10^{-8} < \tau_t < 10^{-1}$.

A convergence test was performed to determine the values for numbers of acoustic, N, and structural, M, modes in the calculations with reasonable accuracy before performing the simulation of the active control. The numbers of acoustic and structural modes in the present calculation were set to be $N = 848$ and $M = 30$ in the foregoing calculations. The maximum deviation from the results obtained with $N = 2045$ and $M = 100$ is, in general, less than 0·01 dB. All the calculations were done using MATLAB on a DEC workstation 600 a.u.

3. TOTAL ACOUSTIC POTENTIAL ENERGY ATTENUATION

The performance of active sound transmission control is analyzed in terms of the attenuation of total acoustic potential energy under various combinations of τ_r and τ_t in the present study. The frequency concerned is up to $5\omega_{ac}$.

Figure 3(a) illustrates the PE with $\eta_c = 0{\cdot}12$ and $\varphi = 11{\cdot}84$ for a weakly coupled system (6 mm thick glass panel with $L_{x1} = 1$ m) at frequency $0{\cdot}1\omega_{ac}$ under different combinations of τ_r and τ_t with an external source strength of $\sqrt{4\rho_a c^2/V}$. High sound transmission occurs around $\tau_t = 10^{-4}$ and in the region where $\hat{\omega}_{m=0} \neq 0$ (Figure 2) because of the effective drive of the structural mode, $m = 0$, at low frequency. There are some regions with low PE (bright areas) in Figure 3(a) at some combinations of τ_r and τ_t due to the ineffective transmission of sound energy through the flexible panel. For stronger coupling

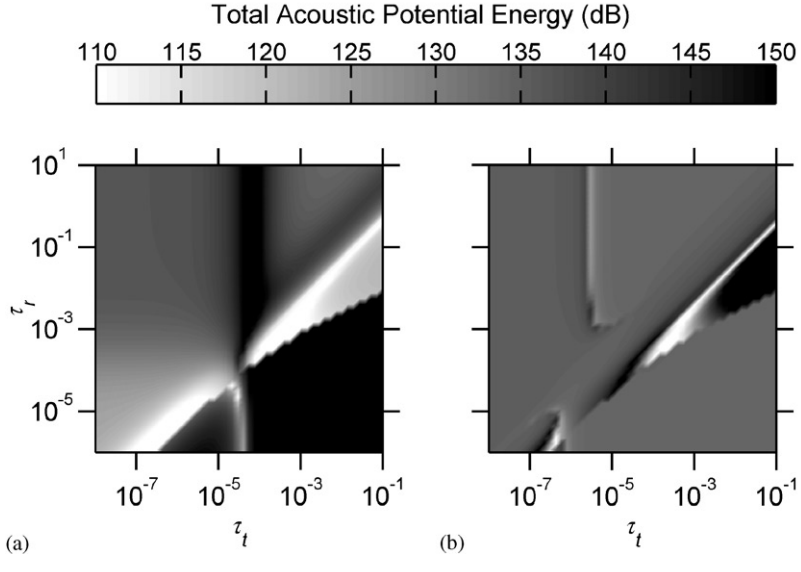

Figure 3. Maps of overall total acoustic potential energy at frequency $0{\cdot}1\omega_{ac}$. (a) $\eta_c = 0{\cdot}12$ and $\varphi = 11{\cdot}84$; (b) $\eta_c = 2{\cdot}93$ and $\varphi = 59{\cdot}22$; $\theta = \pi/4$; all data presented are in dB ref. 10^{-12} N m.

(larger η_c), higher PE transmission is expected as discussed in reference [6]. However, the high PE disappears at strongly coupled system at frequency $0{\cdot}1\omega_{ac}$ for $\eta_c = 2{\cdot}93$ and $\varphi = 59{\cdot}22$ (6 mm thick glass panel with $L_{x1} = 5$ m) as shown in Figure 3(b) because of the high value of φ which results in smaller panel vibration amplitudes at the same driving frequency. Figure 4(a) shows the PE for $\eta_c = 0{\cdot}12$ and $\varphi = 11{\cdot}84$ at frequency $0{\cdot}3\omega_{ac}$ in the ranges of τ_r and τ_t with an external source strength of $\sqrt{4\rho_a c^2/V}$. Peak PE can be observed at some uncoupled eigenfrequencies of the flexible panel (dark lines) besides the small fluctuations of PE over the ranges of τ_r and τ_t in the present study. These uncoupled eigenfrequencies of the flexible panel, which is equal to $0{\cdot}3\omega_{ac}$ with $\varphi = 11{\cdot}84$ and the corresponding edge flexibility coefficients, can be found from the intersection between the planes of $\hat{\omega}_{m=2}$ and $\hat{\omega}\varphi = 3{\cdot}552$ in Figure 2. $\hat{\omega}\varphi$ denotes the forcing frequency normalized by the first cut-off frequency of the simply supported flexible panel. Overall PE transmission is high at the first eigenfrequency of the enclosure as shown in Figure 4(b). Peak PE (dark lines) can be observed at the eigenfrequencies of the flexible panel with $\hat{\omega}_{m=3} = \varphi$ and $\hat{\omega}_{m=4} = \varphi$ (the profile of $\hat{\omega}_{m=3}$ and $\hat{\omega}_{m=4}$ are not shown here). Also, uniform PE transmission can be found at higher frequency at $1{\cdot}5\omega_{ac}$ as shown in Figure 4(c). Peak PE occurs at the eigenfrequency of the panel with $\hat{\omega}_{m=4} = 1{\cdot}5\varphi$. Generally, the PE transmission is uniform in the present τ_r and τ_t range as shown in Figures 3 and 4, except in some regions discussed before.

Figure 5 show the PE attenuation maps for $\eta_c = 0{\cdot}12$ and $\varphi = 11{\cdot}84$ for a weakly coupled system at $0{\cdot}1\omega_{ac}$. For pure vibration control (Figure 5(a)), high effectiveness of PE attenuation can be found for $\tau_t < 10^{-6}$ near the uncoupled eigenfrequency of the flexible panel, $\hat{\omega}_{m=1}$, in Figure 2 (where $\hat{\omega}\varphi = 1{\cdot}184$) and the regions with high-energy transmission in Figure 3(a). The high PE attenuation in the region where $\hat{\omega}_{m=0} \neq 0$ suggests that more effective active control can be achieved for lower structural mode. The performance of pure acoustic control is not as good as that of pure vibration control at low frequency in the present case. However, more uniform PE attenuation can be obtained with various combinations of τ_r and τ_t under the action of a pure acoustic secondary source (Figure 5(b)). Some controllable (dark lines) and uncontrollable (bright lines) structural modes can be observed under this pure acoustic control near the panel-controlled modes. The performance of active sound transmission control using combined vibration and acoustic sources (Figure 5(c)) is similar to that obtained by using pure vibration control (Figure 5(a)). This is also found at lower frequencies, implying that active sound transmission

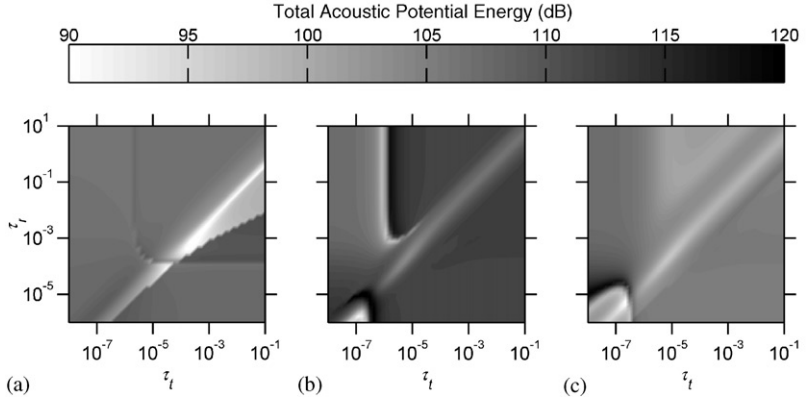

Figure 4. Maps of overall total acoustic potential energy at different frequencies. (a) $0{\cdot}3\omega_{ac}$; (b) ω_{ac}; (c) $1{\cdot}5\omega_{ac}$; $\theta = \pi/4$; $\eta_c = 0{\cdot}12$ and $\varphi = 11{\cdot}84$; all data presented are in dB ref. 10^{-12} N m.

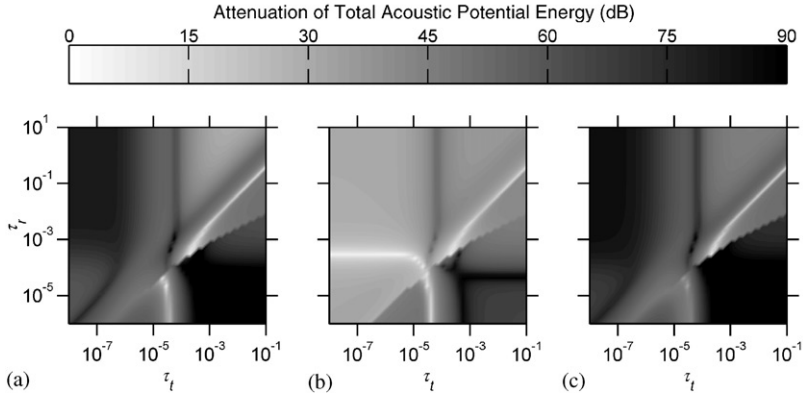

Figure 5. Maps of overall total acoustic potential energy attenuation under potential energy control at frequency $0{\cdot}1\omega_{ac}$: (a) purely vibration control; (b) purely acoustic control; (c) combined vibration and acoustic control. $\theta = \pi/4$; acoustic source at (L_{x_1}, L_{x_2}); force actuator at $(0{\cdot}495L_{x_1}, 0)$; $\eta_c = 0{\cdot}12$ and $\varphi = 11{\cdot}84$.

control using a vibration control source has higher effectiveness as the forcing frequency decreases. Vibration control plays an important role in the combined control source system at frequencies far below the first cut-off frequency of the enclosure.

The effectiveness of PE attenuation under potential energy control using pure vibration control decreases as the frequency increases as shown in Figure 6(a) at $0{\cdot}3\omega_{ac}$. Peak PE attenuation occurs in the region near the two uncoupled eigenfrequencies of the flexible panel, $\hat{\omega}_{m=1}$ and $\hat{\omega}_{m=2}$ (as shown in Figure 2), with small τ_r and τ_t. Ineffective PE attenuation (bright lines in Figure 6(a)) can be found at the uncoupled panel eigenfrequencies (dark lines in Figure 4(a)) using a pure vibration control source. However, pure acoustic control gives slightly better and more uniform performance with various combinations of τ_r and τ_t at $0{\cdot}3\omega_{ac}$ than at $0{\cdot}1\omega_{ac}$ as shown in Figure 6(b) (cf., Figure 5(b)). Also, high PE attenuation is found in the regions of low PE (Figure 4(a)) using a pure acoustic control source as shown in Figure 6(b). It is because the external excitation and also the vibration control source does not effectively drive the vibration of the flexible panel at some combinations of the edge flexibility coefficients, resulting in ineffective vibration control of the flexible panel (Figure 6(a)). This does not apply to acoustic control source. Significant improvement of the performance can be observed using a combined control source scheme as shown in Figure 6(c). The acoustic control in a combined control source system becomes more important as the frequency increases (Figures 5 and 6).

Pure vibration control is obviously not effective at the cavity-controlled mode as shown in Figure 7(a) at ω_{ac}. Nearly, no PE attenuation can be found using a pure vibration control source on the flexible panel with small τ_r or τ_t, while pure acoustic control has comparatively more uniform and high PE attenuation at the cavity-controlled mode (Figure 7(b)). Dramatic increase of the effectiveness of PE attenuation can be observed using combined secondary sources, especially with smaller τ_r or larger τ_t as shown in Figure 7(c). Figure 7(c) also shows high performance of PE attenuation using combined control source at some eigenfrequencies of the flexible panel (cf., Figure 4(b) for $\hat{\omega}_{m=3} = \varphi$ and $\hat{\omega}_{m=4} = \varphi$), which cannot be achieved using either pure vibration or acoustic control (Figures 7(a) and 7(b)).

Poor performance of pure vibration control can also be found at higher frequency with small τ_r or τ_t (for instance, Figure 8(a) at $1{\cdot}5\omega_{ac}$), except at some eigenfrequencies of the

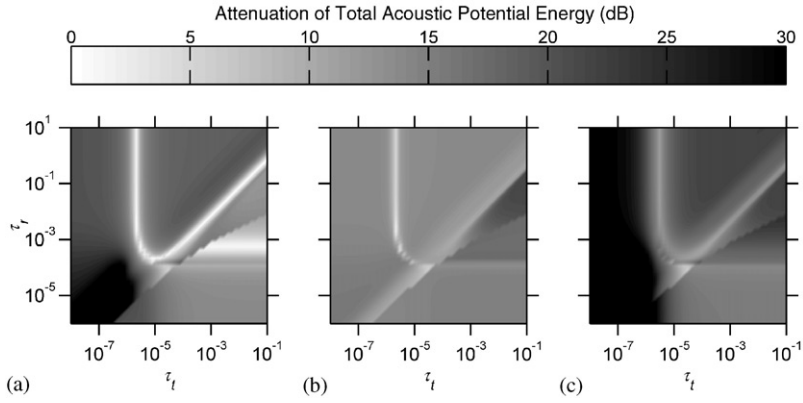

Figure 6. Maps of overall total acoustic potential energy attenuation under potential energy control at frequency $0{\cdot}3\omega_{ac}$. (a) purely vibration control; (b) purely acoustic control; (c) combined vibration and acoustic control; $\theta = \pi/4$; acoustic source at (L_{x_1}, L_{x_2}); force actuator at $(0{\cdot}495L_{x_1}, 0)$; $\eta_c = 0{\cdot}12$ and $\varphi = 11{\cdot}84$.

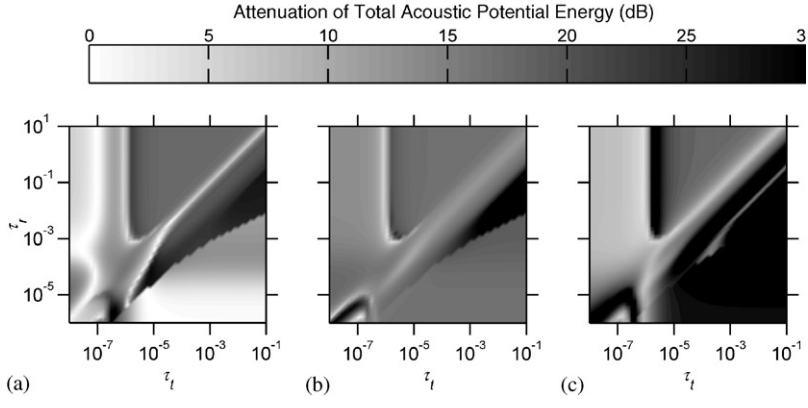

Figure 7. Maps of overall total acoustic potential energy attenuation under potential energy control at frequency ω_{ac}: (a) purely vibration control; (b) purely acoustic control; (c) combined vibration and acoustic control. $\theta = \pi/4$; acoustic source at (L_{x_1}, L_{x_2}); force actuator at $(0{\cdot}495L_{x_1}, 0)$; $\eta_c = 0{\cdot}12$ and $\varphi = 11{\cdot}84$.

flexible panel, which are shown in Figure 4(c) with $\hat{\omega}_{m=4} = 1{\cdot}5\varphi$. Pure vibration control gives nearly no PE attenuation with small τ_r or τ_t at high frequencies. Pure acoustic control can eliminate this weakness of the pure vibration control and maintain a uniform performance of PE attenuation for various combinations of τ_r and τ_t at high frequency as shown in Figure 8(b). The performance of acoustic control source (Figure 8(b)) is similar to that of the combined control source (Figure 8(c)), implying that acoustic control source is more effective than vibration control source at higher frequency, especially near the controllable eigenfrequency of the enclosure in a weakly coupled system. These phenomena of active sound transmission control using pure vibration, pure acoustic and combined control sources can commonly be found at frequencies far from the eigenfrequencies of the enclosure in the present study. However, the magnitudes of sound transmission and PE attenuation are smaller than those near the eigenfrequencies of the enclosure which are not shown here.

Figure 9 shows the PE attenuation maps under potential energy control using a pure vibration, a pure acoustic and combined control sources with $\eta_c = 2{\cdot}93$ and $\varphi = 59{\cdot}22$ at

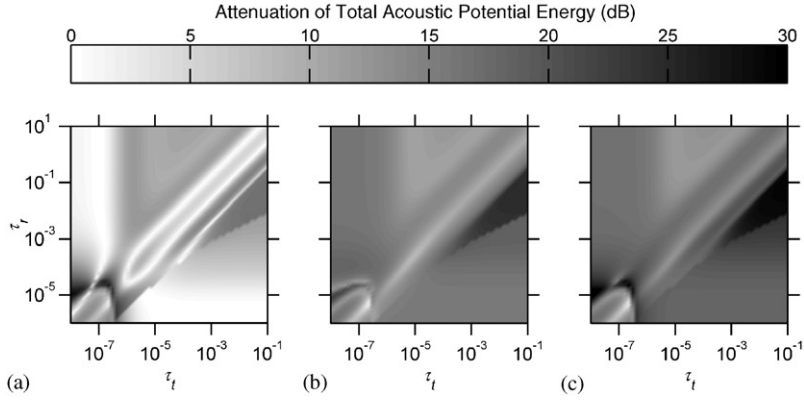

Figure 8. Maps of overall total acoustic potential energy attenuation under potential energy control at frequency $1{\cdot}5\omega_{ac}$: (a) purely vibration control; (b) purely acoustic control; (c) combined vibration and acoustic control. $\theta = \pi/4$; acoustic source at (L_{x_1}, L_{x_2}); force actuator at $(0{\cdot}495L_{x_1}, 0)$; $\eta_c = 0{\cdot}12$ and $\varphi = 11{\cdot}84$.

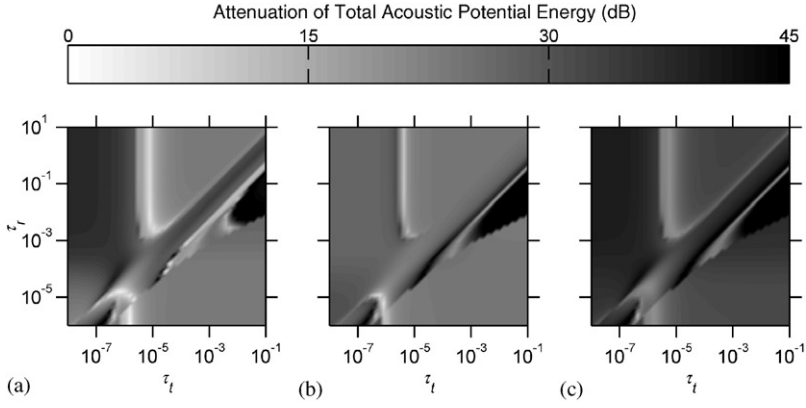

Figure 9. Maps of overall total acoustic potential energy attenuation under potential energy control at frequency $0{\cdot}1\omega_{ac}$. (a) purely vibration control; (b) purely acoustic control; (c) combined vibration and acoustic control; $\theta = \pi/4$; acoustic source at (L_{x_1}, L_{x_2}); force actuator at $(0{\cdot}495L_{x_1}, 0)$; $\eta_c = 2{\cdot}93$ and $\varphi = 59{\cdot}22$.

frequency $0{\cdot}1\omega_{ac}$. Generally, similar results of active sound transmission control, especially for high frequency, can be observed as the strength of the structural–acoustic coupling increases. However, pure acoustic control gives a performance comparable to that under pure vibration control at stronger structural–acoustic coupling and larger value of φ at low frequency as shown in Figure 9(b). The improvement in the performance of acoustic control at stronger structural–acoustic coupling and larger value φ can also be obtained from a combined vibration and acoustic control scheme as shown in Figure 9(c). The attenuation is not dominated by the vibration control as in the weak structural–acoustic coupling system at low frequency (Figure 5). Also, peak PE attenuation using pure vibration, pure acoustic and combined control sources can be found in Figure 9 at the regions of high PE transmission (Figure 3(b)). In addition, ineffective PE attenuation using pure vibration and acoustic controls (shown in Figures 9(a) and 9(b), respectively) at the low PE regions in Figure 3(b) can be eliminated by using the combined control source scheme as shown in Figure 9(c).

For clamped edges, there are no rotation and transverse displacement at the edges and both the flexibilities vanish (i.e., $\tau_r \to 0$ and $\tau_t \to 0$). For simply supported edges, $\tau_r \to \infty$ and $\tau_t \to 0$. It can be observed from Figure 2 that the eigenfrequency of the flexible panel increases from that of the nearly simply supported edges ($\tau_r = 10$ and $\tau_t = 10^{-7}$) as τ_r decreases, while the eigenfrequency of the flexible panel decreases from that of the nearly simply supported edges ($\tau_r = 10$ and $\tau_t = 10^{-7}$) as τ_t increases. As mentioned previously, the difference between the excitation frequency and the controllable eigenfrequencies has crucial impacts on the performance of the active control. One of the examples is shown in Figure 6(a), which shows that PE attenuation increases as both τ_r and τ_t decrease due to a decrease in the difference between the excitation frequency, $0{\cdot}3\omega_{ac}$, and the controllable eigenfrequency of the flexible panel, $\hat{\omega}_{m=1}$. A detailed study on the active control of sound transmission into enclosure with a simply supported panel is given by Lau and Tang [6].

4. CONCLUSIONS

The effects of edge rotational and translational flexibilities of a sound transmitting flexible wall (panel) on the performance of active sound transmission control in a slightly damped rectangular enclosed space are investigated numerically. A compact matrix formulation for a two-dimensional fully structural–acoustic coupled system, where the transmission wall with edges elastically restrained against translation and rotation, under active sound transmission control is derived.

It is found that pure vibration control of the flexible panel is more effective in attenuating sound transmission at some eigenfrequencies of the panel and at frequency lower that the first cut-off frequency of the enclosure. The performance of pure vibration control becomes worse as frequency increases. It is not effective at low rotational or translational flexibility at frequencies higher than the first cut-off frequency of the enclosure. Though better performances of the pure vibration control compared with the pure acoustic control in terms of the total acoustic potential energy attenuation has been found, active sound transmission control using a pure acoustic control source gives a more uniform performance of the total acoustic potential energy attenuation with various combinations of edge rotational and translational flexibility coefficients of the flexible structure. Good performance of pure acoustic control can also be found at some eigenfrequencies of the enclosure and at high frequencies. Pure acoustic control also gives high PE attenuation at some combinations of rotational and translational flexibilities of ineffective transmission of energy, while the pure vibration control does not. Significant improvement in the performance of active sound transmission control is achieved by using combined vibration and acoustic control system as well as proper selection of the edge rotational and translational flexibilities.

ACKNOWLEDGMENTS

The financial supports from the Hong Kong Polytechnic University and the Research Grant Council, HKSAR Government are gratefully acknowledged.

REFERENCES

1. C. R. Fuller and J. D. Jones 1987 *Journal of Sound and Vibration* **112**, 389–395. Experiments on reduction of propeller induced interior noise by active control of cylinder vibration.

2. X. J. Qiu, J. Z. Sha and J. Yang 1995 *Journal of Sound and Vibration* **182**, 167–170. Mechanisms of active control of noise transmission through a panel into a cavity using a point force actuator on the panel.
3. J. Pan, C. H. Hansen and D. A. Bies 1990 *Journal of the Acoustical Society of America* **87**, 2098–2108. Active control of noise transmission through a panel intro a cavity. Part I: Analytical study.
4. J. Pan and C. H. Hansen 1991 *Journal of the Acoustical Society of America* **90**, 1488–1492. Active control of noise transmission through a panel into a cavity. Part II. experimental study.
5. S. M. Kim 1998 *Ph.D. Thesis, University of Southampton*. Active control of stationary random sound fields.
6. S. K. Lau and S. K. Tang 2001 *Journal of the Acoustical Society of America* **110**, 925–938. Sound fields in a rectangular enclosure under active sound transmission control.
7. L. A. Roussos 1985 *NASA Technical Report* 2398. Noise transmission loss of a rectangular plate in an infinite baffle.
8. P. A. A. Laura and R. O. Grossi 1981 *Journal of Sound and Vibration* **75**, 101–107. Transverse vibrations of rectangular plates with edges elastically restrained against translation and rotation.